

# Does blood type affect the COVID-19 infection pattern?

Mattia Miotto,<sup>1,2</sup> Lorenzo Di Rienzo,<sup>2</sup> Giorgio Gosti,<sup>2</sup> Edoardo Milanetti,<sup>1,2</sup> and Giancarlo Ruocco<sup>2,1</sup>

<sup>1</sup>*Department of Physics, University of Rome ‘La Sapienza’, Piazzale Aldo Moro, 5, I00185, Rome, Italy*

<sup>2</sup>*Fondazione Istituto Italiano di Tecnologia (IIT), Center for Life Nano Science, Viale Regina Elena 291, I00161 Roma, Italy*

Among the many aspects that characterize the COVID-19 pandemic, two seem particularly challenging to understand: *i*), the great geographical differences in the degree of virus contagiousness and lethality which were found in the different phases of the epidemic progression, and, *ii*), the potential role of the infected people’s blood type in both the virus infectivity and the progression of the disease. Recently, Breiman *et al.* [1] presented a hypothesis that could shed some light on *i*) and *ii*), specifically, it has been proposed that during the subject-to-subject transfer SARS-CoV-2 conserves on its capsid the erythrocytes’ antigens of the source subject, causing a potential immune reaction in a receiving subject which has previously acquired specific antibodies to the source subject antigens. This implies a blood type-dependent infection rate. The strong geographical dependence of the blood type distribution could be, therefore, one of the factors at the origin of *i*). Here we present an epidemiological deterministic model where the infection rules hypothesized in [1] are taken into account. The comparison of the model outcome with exiting worldwide infection progression data seems to support the Breiman *et al.* hypothesis.

## I. INTRODUCTION

The new infectious coronavirus disease 2019, called COVID-19, began to spread from China in December 2019 [2]. The most evident COVID-19 symptoms are pneumonia and respiratory failure, which reiterate the symptoms reported in the SARS (Severe Acute Respiratory Syndrome) epidemic of 2003 [3, 4]. The first cluster to clearly show these symptoms were patients from Wuhan, People’s Republic of China (WMHC) [3]. In early January 2020, scientists at the National Institute of Viral Disease Control and Prevention (IVDC) isolated the new virus for the first time from patients in Wuhan and found it to be a novel  $\beta$ -genus coronavirus, which has been named SARS-CoV-2 [5]. Currently, the outbreak has rapidly spread in many other countries. Hence, on 11 March 2020, the World Health Organization declared it a pandemic [6]. It clearly represents a global threat to public health [7].

Understanding the transmission dynamics of this infection plays a key role in assessing the transmission potential that may be sustained in the future. In this context, models and simulations represent a powerful tool, which can be useful to study and monitor human and animal viral infections [8, 9]. These tools have become fundamental, especially during this pandemic, to evaluate the trade-off between cost and effectiveness of various social distancing strategies, and to enable policymakers to make the best decisions in the interest of the public health [10].

Nonetheless, each disease is characterized by its specific biological rules, therefore it is essential to consider them in a mathematical model in order to describe real situations. As the virus spreads across the world the pandemic has presented a similar pattern, in all the countries that recorded a significant number of infections. The pattern is made up of a first phase that is characterized by an exponential increase of infections and a later phase in

which the implementation of social distancing measures reduces the spread of the disease to a sub-exponential growth, which generally is followed by a gradual decrease of daily infections. Eventually, the gradual decrease in the number of daily infections becomes smaller than the daily recovered number, thus the number of the total infected starts decreasing.

Even if this general pattern has been reproduced around the world, the spread of the virus showed important local differences, mostly in the rate of the initial exponential spread. Given the unrepeatability of this historic event, it is extremely difficult to understand if these patterns are the consequence of geographical inhomogeneities or if these are spurious correlations which are caused by the singularity of the observed event.

Indeed, some works underlined as in the early stage of the epidemics the virus showed a geographical pattern with most of the infection localized in temperate regions characterized by specific characteristics of temperature and humidity [11–14].

Furthermore, in the specific context of Italy, a non-negligible difference in the rate of infection and mortality between the Northern and Southern regions was reported. But most analyses considered these differences as the effect of the implementation of social distancing rules before that the disease spread in South Italy and not of climate variables [15].

Other potential co-morbidities that may explain local patterns are hypertension, obesity, and age distribution, which are known to display heterogeneous local distributions [16, 17].

Recently, Zhao *et al.* [18] found that ABO blood groups presented a different risk to contract COVID-19 as a result of being exposed to SARS-CoV-2. Previously, for the similar coronavirus SARS-CoV responsible for SARS, Guillon *et al.* [19] showed experimentally that for SARS-CoV synthesized by cells that expressed the

A histo-blood group antigen, the interaction between S protein and its membrane receptor, ACE2, could be blocked by anti-A blood group antibodies. Starting from these experimental results regarding the SARS-CoV spike, Breiman *et al.* [1] extend the hypothesis to the new SARS-CoV-2, suggesting that the different susceptibility of individuals with different ABO blood groups may have the same explanation. This new hypothesis, based on the infection rules schematically illustrated in Figure 1, may explain a part of the variability in the infection contagiousness among the countries of the world [1].

Here, we discuss the spread of the epidemic from a mathematical modeling perspective, taking into account the influence of the different sub-populations divided according to the two most important blood group systems, i.e ABO and Rh, in the different geographical areas. The main purpose of this work is to verify whether the hypothesized blood group based infection rules can be consistent with the acquired country-level data on blood group distribution and infection diffusion dynamics.

In the last decades, the modeling of epidemic diffusion behaviors has rapidly developed and found wide application [20]. Many recent papers described different aspects of the COVID-19 disease evolution through mathematical models [21–28]. We propose here a generalization of the widely-used Susceptible-Infected-Recovered model (SIR), a simple compartmental model, where the population is divided into three sets. “Susceptible” are healthy individuals who can be infected by other individuals. “Infected” individuals are those who contracted the virus at time  $t$ , while “Recovered” consists of all the immune individuals, therefore they cannot be infected again. Each of these compartments is time-dependent, owing to the progressive nature of the disease. If we take a deterministic system, we can model the epidemic process using ordinary differential equations. Consequently, the state of each compartment, at any time of the evolution of the system, is completely determined by the initial conditions along with the differential equations [29].

Here, we modified the SIR model to take into account the proposed blood type infection rules with the aim of testing the working hypothesis against real data.

## II. MODELS

In this section we first briefly consider the standard SIR model for the time evolution of the fraction of susceptible ( $x(t)$ ), infected ( $y(t)$ ) and recovered ( $z(t)$ ) people in a population of size  $N$ , recalling the main features of the model and its solution.

We then analyze in detail the generalization of the SIR model to a more complex pattern of infection, as the one described in the previous section.

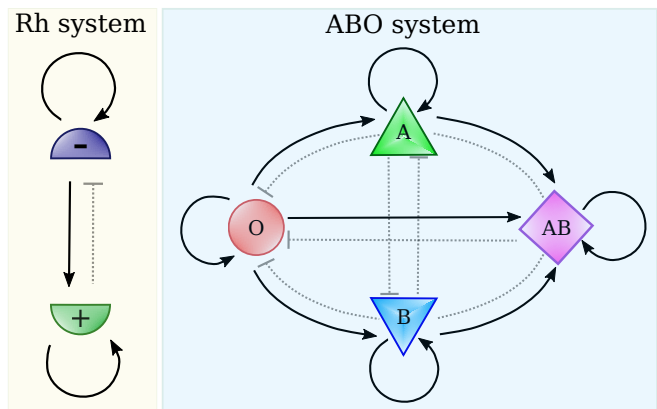


FIG. 1: Scheme of the proposed infection rules according to Rh blood types and ABO ones. Full line connection indicated the possibility of infection,  $W_{ij} = 1$ , while dotted connection its impossibility. In the Rh infection system, individuals of the same group can infect each other, people with the Rh-group can transmit the infection to people with Rh+ one, but not *viceversa*. The scenario of the ABO system is similar although richer. For instance, O type can infect the A type, while the opposite is not possible.

### A. Standard SIR model

The standard SIR model reads

$$\frac{dx(t)}{dt} = -\beta x(t) y(t) \quad (1)$$

$$\frac{dy(t)}{dt} = \beta x(t) y(t) - \gamma y(t) \quad (2)$$

$$\frac{dz(t)}{dt} = \gamma y(t) \quad (3)$$

where the three functions satisfy the relation

$$x(t) + y(t) + z(t) = 1 \quad (4)$$

and the parameter  $\beta$  and  $\gamma$  represent the infection and recovery rate respectively.

We introduce the parameter  $\rho \doteq \gamma/\beta$  and the re-scaled time  $\tau \doteq \beta t$ . We thus chose the simple and realistic case of a few infected persons at time zero, and all the remaining population susceptible of infection:

$$\begin{aligned} x(0) &= x_o \\ y(0) &= y_o = 1 - x_o \\ z(0) &= 0. \end{aligned} \quad (5)$$

The solution of the standard SIR model that obey these initial conditions can be written as:

$$x(\tau) = x_o e^{-z(\tau)/\rho} \quad (6)$$

$$y(\tau) = 1 - z(\tau) - x_o e^{-z(\tau)/\rho} \quad (7)$$

$$\tau = \frac{1}{\rho} \int_0^{z(\tau)} \frac{d\zeta}{1 - \zeta - x_o e^{-\zeta/\rho}}. \quad (8)$$

### 1. Short time expansion

It is well known that the onset of the infection is well represented by an exponential growth. It is therefore useful to perform the expansion of the solutions (6), (7) and (8) for  $\tau \rightarrow 0$ .

In the small  $\tau$  limit, the expression for  $\tau(z)$  given by Eq. (8), becomes:

$$\tau(z) \approx \tau|_{z=0} + \left. \frac{d\tau}{dz} \right|_{z=0} z = \frac{1}{\rho} \frac{z}{(1-x_o)},$$

thus

$$z(\tau) \approx \rho(1-x_o)\tau = \rho y_o \tau. \quad (9)$$

By substituting in (6) and (7), we get

$$x(\tau) \approx x_o e^{-y_o \tau} \quad (10)$$

$$y(\tau) \approx 1 - \rho y_o \tau - x_o e^{-y_o \tau}. \quad (11)$$

The last equation, by expanding the exponential, collecting the terms linear in  $\tau$  and resumming the exponential, becomes:

$$y(\tau) \approx y_o e^{(x_o - \rho)\tau} \quad (12)$$

which represents the desired exponential growth of the infection at short time. As at short time the fraction of infected population is very small (i.e.  $y_o \ll 1$ ), we can safely approximate  $x_o \approx 1$ :

$$y(\tau) \approx y_o e^{(1-\rho)\tau}. \quad (13)$$

Equation (13) expresses one of the key concepts of epidemic models. The number of infectious individuals grows exponentially if  $\rho < 1$ , or  $\beta > \gamma$ . Often, in the literature, the parameter controlling the level of infection growth is the ‘‘reproduction number’’,  $R_o$ , defined as the average number of secondary infections caused by a primary case introduced in a fully susceptible population [30].  $R_o$  is therefore equal to  $\beta/\gamma$ , which, in our notation, means  $R_o = 1/\rho$ .

From those simple considerations arises the concept of epidemic threshold: only if  $(1-\rho) > 0$ , thus  $R_o > 1$  (i.e. if a single infected individual generates on average more than one secondary infection), an infective agent can cause an outbreak. If  $R_o < 1$  (i.e. if a single infected individual generates less than one secondary infection), then  $(1-\rho) < 0$  and the onset of the epidemic is characterized by a *decreasing* number of cases.

### 2. Summary of standard SIR properties

In this subsection, we recollect the main results from Sections IIA1. The main results are four. First, it is

worth to always perform the limit  $x_o \rightarrow 1$ , while keeping  $y_o \neq 0$  as discussed below. This allows us to correctly capture the exponential growth that characterizes the initial phase of an epidemic.

Second, the exact solutions of the standard SIR model with the initial conditions (5) are:

$$x(\tau) = e^{-z(\tau)/\rho}$$

$$y(\tau) = 1 - z(\tau) - e^{z(\tau)/\rho}.$$

$$\tau = \frac{1}{\rho} \int_0^{z(\tau)} \frac{d\zeta}{1 - \zeta - e^{-\zeta/\rho}}$$

Third, the value of maximum infection is found to be:

$$y_M = 1 - \rho + \rho \log(\rho).$$

Fourth, at short time, when the exponential growth dominates the solution, the following approximations hold:

$$x(\tau) = e^{-y_o \tau}$$

$$y(\tau) = y_o e^{(1-\rho)\tau} \quad (14)$$

$$z(\tau) = \rho y_o \tau$$

As last observation, it is worth to emphasize that Eq. (14) is identical to the short time expansion of the infectivity in the SIS (Susceptible-Infected-Susceptible) model, which is a simplified version of the SIR model where individuals never acquire immunity to the infection. The latter, at short time, reads:

$$\dot{y}(\tau) = x_o y(\tau) - \rho y(\tau) \quad (15)$$

whose solution coincides with Eq. (12) or, after the  $x_o = 1$  approximation, with Eq. (13)).

## B. Generalized SIR model

Our aim is to generalize the SIR model to the case where the population is not homogeneous, but it is composed of different sub-populations that follow specific infection rules.

In the general case of  $k$  sub-populations  $i = 1, \dots, k$ , the time evolution of the variables can be written as:

$$\dot{x}_i = -x_i \sum_{j=1}^k W_{ij} y_j \quad (16)$$

$$\dot{y}_i = x_i \sum_{j=1}^k W_{ij} y_j - \rho y_i \quad (17)$$

$$\dot{z}_i = \rho y_i \quad (18)$$

where the matrix  $\mathbf{W}$  encodes the infection rules.

As an example, we discuss the simple case of only two sub-populations that could follow the infection rules associated to the Rh $\pm$  blood type ( $f_1 \equiv f_-$ ,  $f_2 \equiv f_+$ , where

$f_{\pm}$  is the frequency of one blood type in the population). The sub-population with Rh+, according to the working hypothesis, cannot infect the Rh- one. On the other hand, the Rh- sub-population can infect both Rh- and Rh+ sub-populations. The matrix  $\mathbf{W}^{(2)}$  in this situation turns out to be:

$$\mathbf{W}^{(2)} = \begin{pmatrix} 1 & 0 \\ 1 & 1 \end{pmatrix} \quad (19)$$

The corresponding SIR equations, to our knowledge, cannot be solved by quadrature. The numerical solution for this  $k = 2$  case is also depicted in Figure 2, where as an example the fraction of infected people  $y_i(\tau)$  for the two sub-populations (green dashed and red dotted lines) and the total fraction  $y_T(\tau)$  of infected people (blue line) are reported as a function of the reduced time  $\tau$  for the case  $\rho = 0.1$  and  $f_1 = 0.4$ ,  $f_2 = 0.6$ .

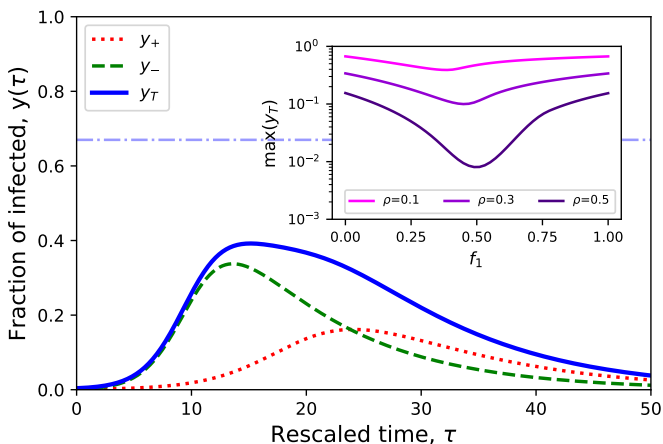


FIG. 2: Example of numerical solution of the generalised SIR model for two sub-populations ( $k = 2$ ) and for the infectivity matrix of Eq. (19). The reported example is for  $\rho = 0.1$ ,  $f_1 = 0.4$  and  $f_2 = 0.6$ . The dashed and red lines represent the fraction of infected people in the two sub-populations, the blue line the total fraction of infected persons, the horizontal dotted line indicates the maximum value,  $y_M$ , of  $y_T(\tau)$  in the case of all-infect-all rule. The inset report the maximum of  $y_T(\tau)$  as a function of  $f_1$  ( $f_2 = 1 - f_1$ ) for three distinct values of  $\rho$ .

One can immediately notice that the maximum fraction of infected people,  $y_M$ , is reduced with respect to the one-population case (horizontal dash-dotted blue line). This is a trivial consequence of the impossibility of Rh+ to infect Rh-, thus reducing the “effective” infection rate. The dependence of the maximum infectivity on  $f_1$  ( $f_2 = 1 - f_1$ ) is reported in the inset of Figure 2 for three representative values of  $\rho$  ( $\rho=0.1$ , 0.3 and 0.5). Noteworthy, for the case  $\rho=0.5$ , i.e.  $R_0=2$ , the actual value observed in Europe, the maximum of infectivity is reduced from the all-infect-all case ( $\approx 0.2$ ) to a value more than ten times smaller ( $\approx 0.01$ ) when  $f_1$  approach 0.5.

The immediate consequence of this finding is that the time evolution of the epidemic strongly depends on the

blood type distribution, giving a qualitative explanation of the observed high geographical variability: even a small change in  $f_1/f_2$  highly affects both the infectivity maximum and the infectivity growth rate in the initial exponential growth phase.

If we consider the effects of the ABO types only, and we neglect the Rh $\pm$  blood difference, we have four sub-populations with the corresponding frequencies:  $f_1 \equiv f_0$ ,  $f_2 \equiv f_A$ ,  $f_3 \equiv f_B$ ,  $f_4 \equiv f_{AB}$ . With the infection rules summarised in Figure 1 the  $\mathbf{W}^{(4)}$  matrix results:

$$\mathbf{W}^{(4)} = \begin{pmatrix} \mathbf{W}^{(2)} & \mathbf{0} \\ \mathbf{W}^{(2)} & \mathbf{W}^{(2)} \end{pmatrix} \quad (20)$$

Finally, in the case where both the ABO and the Rh types play a role, there are eight subpopulations with respective frequencies  $f_{O-} \equiv f_1$ ,  $f_{A-} \equiv f_2$ ,  $f_{B-} \equiv f_3$ ,  $f_{AB-} \equiv f_4$ ,  $f_{O+} \equiv f_5$ ,  $f_{A+} \equiv f_6$ ,  $f_{B+} \equiv f_7$ ,  $f_{AB+} \equiv f_8$ , and the corresponding matrix  $\mathbf{W}^{(8)}$  reads:

$$\mathbf{W}^{(8)} = \begin{pmatrix} \mathbf{W}^{(4)} & \mathbf{0} \\ \mathbf{W}^{(4)} & \mathbf{W}^{(4)} \end{pmatrix} \quad (21)$$

The recursive structure of Eqs. (19 - 21) has a simple explanation, that can be better understood if we think of the ABO blood type system as the combination of two codominant and one recessive allele that form two independent systems. Let’s specify if a person does have (“+”) or does not have (“-”) the antigen A (A+ or A- respectively), analogously for the antigen B (B+ or B-). Then the usual blood type is:  $0 \equiv [A-, B-]$ ;  $A \equiv [A+, B-]$ ;  $B \equiv [A-, B+]$ ;  $AB \equiv [A+, B+]$ . With this notation it is clear that the “ABO” system (which follows  $W^{(4)}$ ) is the product of the “A” system (which follows  $W^{(2)}$ ) and the “B” system (which again follows  $W^{(2)}$ ):  $ABO = A\pm \times B\pm$ . Furthermore, by multiplying the ABO system by the Rh $\pm$  system we get the  $ABO \times Rh\pm = A\pm \times B\pm \times Rh\pm$  system, which obeys the  $W^{(8)}$  infection rules. Summing up, any time it exists a set of antigens,  $A_i$ ,  $i = 1..a$ , that can be either present or absent, the infection rule of the  $A_1 \times A_2 \times \dots \times A_a$  system follows the  $W^{(k)}$  infection rule with  $k = 2^a$ .

The set of  $3k$  differential equations (16 - 18), together with the initial conditions:

$$\begin{aligned} x_i(0) &= f_i x_o \approx f_i \\ y_i(0) &= f_i y_o \\ z_i(0) &= 0 \end{aligned} \quad (22)$$

and the sum rule

$$\sum_{i=1}^k f_i = 1 \quad (23)$$

allows one to work out the short time expansion for the infected person fraction on each of the  $k$  sub-populations:

$$y_i(\tau) = y_o f_i e^{\pi_i^{(k)} \tau} \quad i = 1, \dots, k \quad (24)$$

with

$$\pi_i^{(k)} = \sum_j W_{ij} f_j - \rho = (\mathbf{W} \cdot \bar{f})_i - \rho \doteq p_i^{(k)} - \rho, \quad (25)$$

as well as the total number of infected persons:

$$y_T(\tau) = \sum_i y_i(\tau) = y_o e^{\pi_T^{(k)} \tau} \quad i = 1, \dots, k \quad (26)$$

with

$$\pi_T^{(k)} = \sum_i \sum_j f_i W_{ij} f_j - \rho = \bar{f} \cdot \mathbf{W} \cdot \bar{f} - \rho \doteq p_T^{(k)} - \rho \quad (27)$$

which implicitly define  $p_i^{(k)}$  and  $p_T^{(k)}$ . This simple expression for the inverse of the characteristic time of the infection at its onset is the sum of two terms:  $\pi_T^{(k)} = p_T^{(k)} - \rho$ .

The first one,

$$p_T^{(k)} \doteq \bar{f} \cdot \mathbf{W} \cdot \bar{f} \quad (28)$$

depends only on the abundance of the sub-population ( $\bar{f}$ ) and on the infection rules ( $\mathbf{W}$ ), the second ( $\rho = \gamma/\beta$ ) on the overall recovery and infection rates of populations.

To study the global effect of the population composition on the progression of the infection, we concentrate on the term  $p_T^{(k)}$  which acts as a ‘‘susceptibility’’.

It is worth to note that, for any  $k$ , the susceptibility is maximum when  $\bar{f} = (0, \dots, 0, 1, 0, \dots, 0)$ ,  $p_T^{(k)} = 1$ , i.e. when one sub-population fraction dominates, while it minimum when the sub-populations are all of the same size:  $\bar{f} = (1/k, 1/k, \dots, 1/k)$ . In the latter case, for the infection rules reported before,  $p_T^{(k)} = (3/4)^{(k/2)}$ . Thus the susceptibility decreases on increasing the number of sub-populations and decreases on equalizing their abundances.

Infection rules and compositions of the population are expected to shape the infection dynamics along with the usual infection and recovering rates.

In the following we will analyze some datasets of individuals infected by SARS-CoV-2, stratified by ABO and ABO×Rh blood types. Then, we will deal with the contagion curves of a large set of countries and try to assess whether the present model could represent the real outcome of the COVID-19 pandemics.

Specifically, we will first compare data collected in the Chinese regions of Wuhan and Shenzhen reported in [18], in the Ankara region (Turkey) [31], and in New York City (NY, USA) [32], where the ABO type of sets of infected people have been determined (ABO×Rh in the New York City case). This allows for a direct comparison between our model predictions and real data. Then we move to analyze the early stages of the infection in different countries at a worldwide level. To take into account differences like lifestyle, climate, geographic location, and other factors that likely influence the epidemics rates as well, we identified four major areas, i.e. Europe, Asia, Africa, and South America.

### III. MATERIALS AND METHODS

#### A. Cases where infection data are stratified by blood type

##### 1. Wuhan/Shenzhen case

The first analysis of this work is carried out on the data from [18], which reports the abundance of each ABO blood group on the local population and the Covid-19 patients. These data are schematically reported in Table I for three sub-cases (two Wuhan hospitals and one Shenzhen hospital). The number of patients in the three sub-cases are 1775, 113, and 285, respectively.

TABLE I: Data from reference [18] used to determine the quantities plotted in Figure 3:  $\ln(d_i/f_i)$  and  $p_T^{(4)}$  following Eq. (25), with  $d_i$  being the fractions of infected having blood group  $i$ ,  $f_i$  is the fraction of population with blood group  $i$  and  $p_T^{(4)}$  represent the susceptibility of the population to become infected.

Dataset	Quantity	O	A	B	AB
Wuhan 1	$f_i$	0.3384	0.3216	0.2490	0.0910
	$d_i$	0.2580	0.3775	0.2642	0.1003
Wuhan 2	$f_i$	0.3384	0.3216	0.2490	0.0910
	$d_i$	0.2478	0.3982	0.2212	0.1330
Shenzhen	$f_i$	0.3877	0.2877	0.2511	0.0742
	$d_i$	0.2842	0.2877	0.2912	0.1368

##### 2. Ankara case

Further data stratified by ABO blood groups are reported in [31] for 186 patients with a confirmed diagnosis of COVID-19 in the region of Ankara. The fraction of infected,  $d_i$  for each ABO blood group are reported in Table II, together with the frequencies of the groups in a control sample of 1881 healthy individuals, whose blood groups were collected in the same period of time of the 186 infected cases. The reduced size of the sample assures statistical confidence only for A and O groups (p-value < 0.05), with AB being the less trust-worth with a p-value of 0.364 (see [31]).

TABLE II: Data from reference [31] used to determine the quantities plotted in Figure 4:  $\ln(d_i/f_i)$  and  $p_T^{(4)}$  following Eq. (25), with  $d_i$  being the fractions of infected having blood group  $i$ ,  $f_i$  is the fraction of population with blood group  $i$  and  $p_T^{(4)}$  represent the susceptibility of the population to become infected.

Quantity	O	A	B	AB
$f_i$	0.3725	0.3804	0.1473	0.0998
$d_i$	0.2473	0.5699	0.1075	0.0753



### 3. New York City case

The previous cases provided data of infected individuals stratified by ABO groups, i.e. no further division by Rhesus groups was reported. A recent work by Zitz et al. [32], collected information of both ABO and Rh± groups for 682 infected individuals tested in New York Presbyterian/Columbia University Irving Medical Center (NYP/CUIMC). We summarized the information relevant for our analysis in Table III. Due to both the relatively small size of the sample and the lower frequencies of Rh-negative blood groups in the local population, data for Rh-negative groups are affected by a higher statistical error with respect to Rh-positive one. In particular, no infected individuals with group AB- were found by [32]. Thus, we restricted our analyses to only seven groups (i.e.  $O_+, O_-, A_+, A_-, B_+, B_-, AB_+$ ).

TABLE III: Data from reference [32] used to determine the quantities plotted in Figure 5:  $\ln(d_i/f_i)$  and  $p_T^{(8)}$  following Eq. (25), with  $d_i$  being the fractions of infected having blood group  $i$ ,  $f_i$  is the fraction of population with blood group  $i$  and  $p_T^{(8)}$  represent the susceptibility of the population to become infected considering both ABO and Rh infection rules.

Quantity	O+	A+	B+	AB+	O-	A-	B-	AB-
$f_i$	0.437	0.296	0.136	0.038	0.044	0.032	0.013	0.004
$d_i$	0.427	0.317	0.160	0.031	0.031	0.025	0.010	-

### 4. Data Analysis

Once we have collected the available data on the number of infected people stratified by blood type,  $d_i$ , in a geographical area where the blood type distribution,  $f_i$ , is known we perform the comparison of these data with the model. According to Eqs. (24) and (27) we expect that

$$d_i = y_o f_i e^{(p_i^{(k)} - \rho)\tau^*} \quad i = 1..k \quad (29)$$

with  $p_i^{(k)} = (\mathbf{W} \cdot \bar{f})_i$  and  $\tau^*$  the specific (reduced) time when the data have been collected. Therefore

$$\ln(d_i/f_i) = K + p_i^{(k)} \tau^* \quad i = 1..k \quad (30)$$

being  $K$  a constant ( $K = \ln y_o - \rho\tau^*$ ) not depending on  $i$ . We thus expect a linear relation between  $\ln(d_i/f_i)$  and  $p_i^{(k)}$ . The error bars on  $\ln(d_i/f_i)$  are one standard deviation calculated by assuming a Poissonian distribution for the number of cases, thus  $\Delta(\ln(d_i/f_i)) = 1/\sqrt{n_i}$  being  $n_i$  the number of infected persons with blood type  $i$ .

#### B. Cases where infection data are not stratified by blood type

To our knowledge, the only studies reporting the blood type stratification of the infection data are discussed be-

low. To make further tests on the blood type constrained infection rules proposed in [1], we have to abandon  $p_i^{(k)}$  (the susceptibility per group) and focus on  $p_T^k$  (the total susceptibility), for which a large amount of data is available.

#### 1. The countries case

The incidence of the different blood types in different nations can be found in Wikipedia [33], where a collection of data and the original sources references are reported. These frequencies  $f$  are also listed in Table IV, together with the country ISO code.

From these data we can calculate  $p_T^{(2)}$  (keeping into account only the Rh± type),  $p_T^{(4)}$  (keeping into account only the ABO type) and  $p_T^{(8)}$  (keeping into account both the Rh± and the ABO types) according to Eq. (27) for each country. To estimate the uncertainty on  $p_T^{(k)}$ , we observe that the  $f$  are reported with three significant digits. We therefore associate to each  $f$  (which value is of the order of one) an error equal to  $\Delta f = 10^{-3}$ , and we estimate the upper limit of the error on  $p_T^{(k)}$ , which is bi-linear in  $f$ , as  $\Delta p_T^{(k)} \approx 2\sqrt{k}\Delta f$ .

The data of the contagion by country is taken from World Health Organization (WHO) Coronavirus Disease (COVID-19) Dashboard on date 12th of June 2020 [34]. To ensure statistical reliability, we selected only countries that had registered at least 2000 positive cases from the start of the epidemic. Requiring also to know the frequencies of both ABO and Rh±, we ended up with 78 countries, whose information is reported in Table IV.

In particular, the WHO data reports the number of new infections per day,  $\dot{D}(t)$ . From this quantity, we easily obtain the cumulative number of people that have been infected as a function of time,  $D(t) = \int_0^t \dot{D}(t') dt'$ . The cumulative, rather than directly with  $\dot{D}(t)$  allows us to work on cleaner and more solid data, because the day-by-day fluctuations are averaged out in the long run. Coming back to the model, at short times the cumulative  $D_T(\tau)$  is directly related to  $y_T(\tau)$ , which short-time expansion is reported in Eq. (26). Overall, the COVID19 infection is characterized by low mortality but a high infectivity rate together with both long incubation and recovery periods. These conditions assure that limiting our analysis to the early stages of the infection, the cumulative can be regarded as a good proxy for the number of infected.

For each country reported in Table IV, we manually selected the time interval corresponding to the onset of the infection. In that range, we performed an unsupervised fit using the function:

$$Y(t) = \begin{cases} m_0 t & \text{if } t < t_0 \\ m_0 t_0 + A (e^{m(t-t_0)} - 1) & \text{if } t > t_0 \end{cases} \quad (31)$$

TABLE IV: Percentages of blood groups ( $f_i$ ) as reported in [33], susceptibility,  $p_T^{(k)}$  as given by Eq. (27), and inverse characteristic time,  $m$ , of the exponential phase of the infection for the analysed countries as derived for the fit to the observed data.

Country	Cluster	Code	$O_+$	$A_+$	$B_+$	$AB_+$	$O_-$	$A_-$	$B_-$	$AB_-$	$p_T^{(2)}$	$p_T^{(4)}$	$p_T^{(8)}$	$m$	$\Delta m$	$R^2$
Argentina	SA	AR	45.40	34.26	8.59	2.64	8.40	0.44	0.21	0.06	0.917	0.679	0.635	0.196	0.011	0.98
Armenia	AS	AM	29.00	46.30	12.00	5.60	2.00	3.70	1.00	0.40	0.934	0.618	0.577	0.143	0.025	0.97
Australia	AU	AU	40.00	31.00	8.00	2.00	9.00	7.00	2.00	1.00	0.846	0.660	0.556	0.223	0.005	0.99
Austria	EU	AT	30.00	37.00	12.00	5.00	6.00	7.00	2.00	1.00	0.866	0.612	0.530	0.216	0.033	0.98
Bahrain	AS	BH	48.48	19.35	22.61	3.67	3.27	1.33	1.04	0.25	0.945	0.635	0.600	0.356	0.054	0.97
Bangladesh	AS	BD	29.45	26.01	33.66	8.29	0.95	0.67	0.70	0.27	0.975	0.553	0.539	0.245	0.008	1.00
Belgium	EU	BE	38.00	34.00	8.60	4.10	7.00	6.00	1.50	0.80	0.870	0.647	0.564	0.209	0.019	0.99
Bolivia	SA	BO	51.53	29.45	10.11	1.15	4.39	2.73	0.54	0.10	0.928	0.680	0.631	0.148	0.012	0.95
Bosnia and Herzegovina	EU	BA	31.00	36.00	12.00	6.00	5.00	7.00	2.00	1.00	0.872	0.609	0.530	0.152	0.010	0.99
Brazil	SA	BR	36.00	34.00	8.00	2.50	9.00	8.00	2.00	0.50	0.843	0.653	0.552	0.272	0.015	0.98
Bulgaria	EU	BG	28.00	37.00	13.00	7.00	5.00	7.00	2.00	1.00	0.872	0.600	0.524	0.063	0.038	0.97
Cameroon	AF	CM	42.80	38.80	12.00	3.30	1.40	1.20	0.40	0.10	0.970	0.636	0.617	0.400	0.059	0.95
Canada	NA	CA	39.00	36.00	7.60	2.50	7.00	6.00	1.40	0.50	0.873	0.661	0.578	0.250	0.016	0.96
Chile	SA	CL	85.50	8.70	3.35	1.00	1.20	0.10	0.05	0.10	0.986	0.877	0.865	0.411	0.034	0.97
China	AS	CN	47.70	27.80	18.90	5.00	0.28	0.19	0.10	0.03	0.994	0.620	0.617	0.419	0.069	1.00
Colombia	SA	CO	61.30	26.11	2.28	1.47	5.13	2.70	0.70	0.31	0.919	0.754	0.692	0.218	0.015	0.97
Croatia	EU	HR	29.00	36.00	15.00	5.00	5.00	6.00	3.00	1.00	0.872	0.588	0.513	0.159	0.017	0.99
Cuba	SA	CU	45.80	33.50	10.20	2.90	3.60	2.80	1.00	0.20	0.930	0.654	0.608	0.220	0.020	0.95
Czechia	EU	CZ	27.00	36.00	15.00	7.00	5.00	6.00	3.00	1.00	0.872	0.583	0.511	0.287	0.029	0.98
Congo	AF	CD	59.50	21.30	15.20	2.40	1.00	0.30	0.20	0.10	0.984	0.685	0.674	0.123	0.010	0.99
Denmark	EU	DK	35.00	37.00	8.00	4.00	6.00	7.00	2.00	1.00	0.866	0.643	0.555	0.320	0.049	0.99
Dominican Republic	SA	DO	46.20	26.40	16.90	3.10	3.70	2.10	1.40	0.20	0.931	0.630	0.587	0.295	0.047	0.94
Ecuador	SA	EC	75.00	14.00	7.10	0.50	2.38	0.70	0.30	0.02	0.967	0.802	0.775	0.471	0.028	0.99
Egypt	AF	EG	52.00	24.00	12.40	3.80	5.00	2.00	0.60	0.20	0.928	0.672	0.625	0.158	0.029	0.97
El Salvador	SA	SV	62.00	23.00	11.00	1.00	1.00	1.00	0.70	0.30	0.971	0.706	0.683	0.148	0.007	0.98
Ethiopia	AF	ET	39.00	28.00	21.00	5.00	3.00	2.00	1.00	1.00	0.935	0.593	0.553	0.087	0.002	1.00
Finland	EU	FI	28.00	35.00	16.00	7.00	5.00	6.00	2.00	1.00	0.880	0.584	0.515	0.127	0.007	0.98
France	EU	FR	36.00	37.00	9.00	3.00	6.00	7.00	1.00	1.00	0.872	0.647	0.561	0.251	0.007	0.99
Germany	EU	DE	35.00	37.00	9.00	4.00	6.00	6.00	2.00	1.00	0.872	0.637	0.555	0.230	0.022	0.99
Ghana	AF	GH	53.80	17.60	18.30	2.80	4.50	1.30	1.30	0.20	0.928	0.668	0.624	0.091	0.013	0.98
Greece	EU	GR	37.40	32.90	11.00	3.70	7.00	5.00	2.00	1.00	0.872	0.631	0.551	0.282	0.063	0.94
Guinea	AF	GN	46.88	21.64	22.86	4.52	2.00	0.90	1.00	0.20	0.961	0.621	0.596	0.094	0.005	0.99
Honduras	SA	HN	57.50	27.00	7.80	2.50	2.70	1.70	0.60	0.20	0.951	0.702	0.666	0.128	0.015	0.98
Hungary	EU	HU	27.00	33.00	16.00	8.00	5.00	7.00	3.00	1.00	0.866	0.577	0.500	0.132	0.006	1.00
India	AS	IN	27.85	20.80	38.14	8.93	1.43	0.57	1.79	0.49	0.959	0.565	0.541	0.191	0.005	1.00
Indonesia	AS	ID	36.82	25.87	28.85	7.96	0.18	0.13	0.15	0.04	0.995	0.572	0.569	0.292	0.044	0.97
Iran	AS	IR	33.50	27.00	22.20	7.00	4.00	3.00	2.50	0.80	0.908	0.575	0.522	0.054	0.004	1.00
Iraq	AS	IQ	32.10	25.00	25.60	7.40	3.60	2.70	2.70	0.90	0.911	0.567	0.517	0.092	0.003	1.00
Ireland	EU	IE	47.00	26.00	9.00	2.00	8.00	5.00	2.00	1.00	0.866	0.672	0.578	0.307	0.018	1.00
Israel	AS	IL	32.00	34.00	17.00	7.00	3.00	4.00	2.00	1.00	0.910	0.582	0.528	0.180	0.012	1.00
Italy	EU	IT	39.00	36.00	7.50	2.50	7.00	6.00	1.50	0.50	0.872	0.661	0.577	0.389	0.020	0.99
Ivory Coast	AF	CI	46.50	22.50	22.50	4.30	2.00	1.00	1.00	0.20	0.960	0.619	0.594	0.073	0.016	0.97
Japan	AS	JP	29.90	39.80	19.90	9.90	0.15	0.20	0.10	0.05	0.995	0.570	0.567	0.150	0.023	0.99
Kazakhstan	AS	KZ	30.70	29.80	24.20	8.30	2.30	2.20	1.80	0.70	0.935	0.560	0.524	0.085	0.014	0.98
Kenya	AF	KE	45.60	25.20	21.28	4.20	1.80	1.00	0.90	0.02	0.964	0.614	0.593	0.277	0.045	0.98
Luxembourg	EU	LU	35.00	37.00	9.00	4.00	6.00	6.00	2.00	1.00	0.872	0.637	0.555	0.207	0.022	0.97
Malaysia	AS	MY	34.32	30.35	27.37	7.46	0.17	0.15	0.14	0.04	0.995	0.563	0.560	0.220	0.018	0.96
Mexico	SA	MX	59.09	26.23	8.53	1.73	2.73	1.21	0.40	0.08	0.958	0.708	0.678	0.225	0.031	0.97
Moldova	EU	MD	28.50	31.80	17.60	7.00	5.00	6.00	3.00	1.10	0.872	0.574	0.501	0.168	0.008	0.99
Morocco	AF	MA	42.30	29.80	14.30	4.10	4.50	3.10	1.50	0.40	0.914	0.625	0.572	0.176	0.009	1.00
Nepal	AS	NP	35.20	28.30	27.10	8.60	0.30	0.20	0.20	0.10	0.992	0.567	0.562	0.135	0.025	0.96
Netherlands	EU	NL	39.50	35.00	6.70	2.50	7.50	7.00	1.30	0.50	0.864	0.669	0.577	0.439	0.036	0.99
Nigeria	AF	NG	51.30	22.40	20.70	2.60	1.60	0.70	0.60	0.10	0.971	0.640	0.622	0.155	0.020	0.92
Macedonia	EU	MK	30.00	34.00	15.00	6.00	5.00	6.00	3.00	1.00	0.872	0.588	0.512	0.224	0.034	0.97
Norway	EU	NO	33.20	41.60	6.80	3.40	5.80	7.40	1.20	0.60	0.873	0.661	0.576	0.304	0.047	0.96
Pakistan	AS	PK	26.63	21.60	34.40	9.52	2.17	1.66	3.57	0.45	0.928	0.557	0.518	0.075	0.005	0.99
Peru	SA	PE	70.00	18.40	7.80	1.60	1.40	0.50	0.28	0.02	0.978	0.761	0.744	0.385	0.021	0.99
Philippines	AS	PH	45.90	22.90	24.90	5.97	0.10	0.10	0.10	0.03	0.997	0.608	0.606	0.353	0.027	0.95
Poland	EU	PL	31.00	32.00	15.00	7.00	6.00	6.00	2.00	1.00	0.872	0.594	0.520	0.233	0.022	0.99
Portugal	EU	PT	36.20	39.80	6.60	2.90	6.10	6.80	1.10	0.50	0.876	0.666	0.583	0.389	0.035	0.99
Romania	EU	RO	28.00	36.50	13.60	6.80	5.00	6.50	2.40	1.20	0.872	0.594	0.518	0.184	0.009	0.99
Russian Federation	EU	RU	28.00	30.00	20.00	7.00	4.90	5.80	3.20	1.10	0.872	0.565	0.493	0.185	0.004	1.00
Saudi Arabia	AS	SA	47.80	23.90	17.00	4.00	4.00	2.00	1.00	0.30	0.932	0.638	0.595	0.190	0.037	0.96
Serbia	EU	RS	31.92	35.28	12.60	4.20	6.08	6.72	2.40	0.80	0.866	0.610	0.528	0.143	0.004	1.00
Singapore	AS	SG	44.70	23.90	24.50	5.60	0.60	0.30	0.30	0.10	0.987	0.604	0.596	0.178	0.066	0.98
South Africa	AF	ZA	39.00	32.00	12.00	3.00	6.00	5.00	2.00	1.00	0.880	0.629	0.551	0.208	0.024	0.98
South Korea	AS	KR	27.90	33.87	26.92	10.98	0.10	0.13	0.08	0.02	0.997	0.548	0.546	0.195	0.011	0.97
Spain	EU	ES	35.00	36.00	8.00	2.50	9.00	7.00	2.00	0.50	0.849	0.652	0.558	0.377	0.011	0.99
Sudan	AF	SD	48.00	27.70	15.20	2.80	3.50	1.80	0.80	0.20	0.941	0.642	0.605	0.110	0.003	1.00
Sweden	EU	SE	32.00	37.00	10.00	5.00	6.00	7.00	2.00	1.00	0.866	0.625	0.541	0.303	0.010	0.99
Switzerland	EU	CH	35.00	38.00	8.00	4.00	6.00	7.00	1.00	1.00	0.872	0.650	0.565	0.241	0.044	0.98
Thailand	AS	TH	40.80	16.90	36.80	4.97	0.20	0.10	0.20	0.03	0.995	0.605	0.602	0.270	0.006	0.99
Turkey	AS	TR	29.80	37.80	14.20	7.20	3.90	4.70	1.60	0.80	0.902	0.596	0.538	0.201	0.036	0.98
Ukraine	EU	UA	32.00	34.00	15.00	5.00	5.00	6.00	2.00	1.00	0.880	0.597	0.523	0.229	0.016	0.99
United Arab Emirates	AS	AE	44.10	21.90	20.90	4.30	4.30	2.10	2.00	0.40	0.920	0.618	0.569	0.135	0.007	0.98
United Kingdom	EU	BG	38.00	32.00	8.00	3.00	9.00	7.00	2.00	1.00	0.846	0.653	0.553	0.230	0.008	0.99
United States	NA	US	37.40	35.7												

with  $t_o$ ,  $m_o$ ,  $m$  and  $A$  as free parameters. In this expression,  $A$  is a scaling factor and  $m$  represents the inverse of the characteristic time of the infection exponential growth, which is the quantity that we are looking at. The linear term, observed at the very beginning of the infection curve of different (not all) countries, can be rationalized by assuming that at the very early stage of the infection, people arrive from other countries, spreading the virus before the real exponential growth appears. The constant  $m_o$  is the “arrival rate” of infected people (which is reasonable to assume constant in time), and we do not expect any correlation between  $m$  and  $m_o$ , because  $m$  is an intrinsic characteristic of the population, and  $m_o$  only depend on the arrival from abroad. Besides the specific meaning of the different parameters, our aim is to derive the value of  $m$ , to compare this value with the prediction of the model  $\pi_T^{(k)}$ .

In Table IV, we report the values of  $m$  with its statistical error  $\Delta m$  as derived from the fit.

#### IV. RESULTS

In this section we compare the outcome of the model with the available observational data (presented in the previous section). Here *model* indicates the combination of the generalized SIR (discussed in section II B) and the infection rules hypothesized in [1].

##### A. Cases where infection data are stratified by blood type

###### 1. The Wuhan/Shenzhen case

As first discuss the three cases where the number of infected people is stratified according to the blood type. In two of them (Wuhan/Shenzhen and Turkey) the data are available only for the ABO system, in the third one (New York) the whole set of ABO×Rh types is known.

In the paper of Zhao et al. [18] the data of the Covid-19 contagion are reported, stratified by ABO blood type (no info on the Rh± type are given). In particular, for each of the three investigated hospitals, the authors provide the frequencies of the ABO blood types of the local population,  $\bar{f} = (f_0, f_A, f_B, f_{AB})$  (two of them are the same as the hospitals are in the same city). The authors also report the fraction of cases for each blood ABO type:  $\bar{d} = (d_0, d_A, d_B, d_{AB})$ . These values are summarised in table I.

As discussed before, the model predicts a linear relation between  $\ln(d_i/f_i)$  and  $p_i^{(4)}$ . In Fig. (3) we report a plot of these two quantities. The different colors represent the different datasets. The black line is the result of the least square fitting to all the data. Finally, the light grey indicates the ± one standard deviation area.

The Pearson correlation coefficient for the N=12 data points is 0.87. The corresponding p-value (0.0003) gives

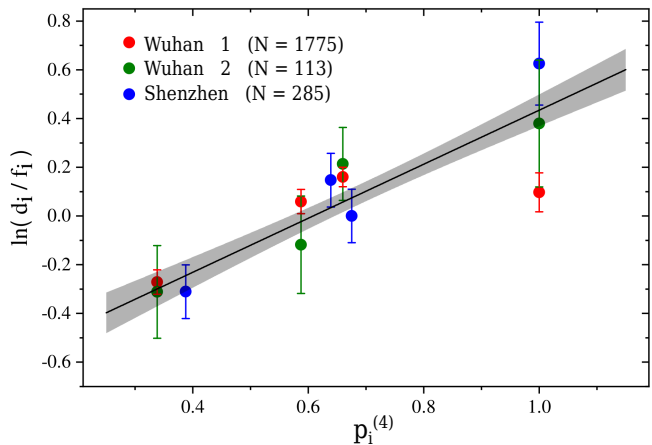


FIG. 3: Ratio between frequencies of infected people for each ABO group,  $d_i$  over frequency of the group on the whole population,  $f_i$  as measured in three hospitals of the Wuhan/Shenzhen region [18] versus its theoretical prediction,  $p_i^{(4)}$  obtained from Eq. (30) using the ABO set of rules and the blood type frequencies in Table I. Black line represents the best solution of a linear fit.

us confidence that the model is compatible with the observations.

###### 2. The Ankara case

The same analysis carried out for the Wuhan/Shenzhen case can be repeated using the Turkish data collected by [31] in the region of Ankara and reported in Table II. Figure 4 shows the logarithm of the ratio between frequencies of infected people for each ABO group,  $d_i$  over frequency of the group on the healthy population,  $f_i$  against the expected susceptibility,  $p_i^{(4)}$ . Although affected by much higher uncertainties with respect to the Chinese counterpart, the behaviour is compatible with that in Figure 3. The Pearson correlation coefficient is 0.34 (N=4, p-value 0.66). The low statistical reliability may be imputable to both the low number of data points and their high uncertainties. Combining the Wuhan/Shenzhen dataset with the Ankara one, we obtained an overall correlation of 0.67 (N=16, p-value 0.004). We note that the AB group seems to deviate from the trend, maybe due to the low number of recorded cases for this group. If the Turkish AB group is not considered in the analysis, the correlation increases up to 0.88 (N=15, p-value  $< 10^{-4}$ ), which is in agreement with the one found for the Wuhan/Shenzhen case alone.

###### 3. The New York case

The data collected by Zeitz *et al.* in New York Presbyterian/Columbia University Irving Medical Center



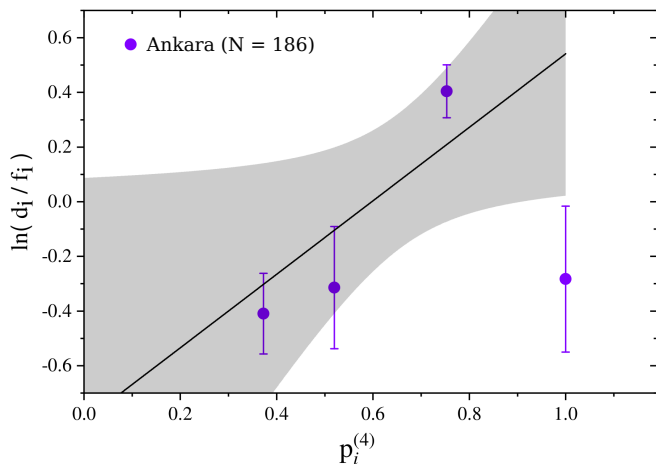


FIG. 4: Ratio between frequencies of infected people for each ABO groups,  $d_i$  over frequency of the group on the whole population,  $f_i$  as measured in a Turkish hospital in the region of Ankara [31] versus its theoretical prediction,  $p_i^{(4)}$  obtained from Eq. (30) using the ABO set of rules and the blood type frequencies in Table II. Black line represents the best solution of a linear fit.

(NYP/CUIMC) hospital [32] are stratified both according to ABO and Rh $\pm$  blood groups. This allows us to test our working hypothesis for the ABO $\times$ Rh set of rules. In Figure 5, the logarithm of the ratio between the number of infected for each group over the group frequency of the local population ( $\ln(d_i/f_i)$ ) is compared with the 8-group susceptibility,  $p_i^{(8)}$  computed according to Eq. 25 and using the data in Table III. The observational data are in good accordance with the theoretical predictions. It is worth emphasizing that the seemingly contradictory behavior of negative Rh groups, and in particular of A-, signaled by [32] is, on the contrary, well accounted for by our model. Computing the Pearson coefficient in this case yields a value of 0.56 with a p-value of 0.19.

Again, as already noted for the Turkish case, the AB group appears to be an outlier. Unfortunately, the collected cases of infected with the AB group are too few to guarantee statistical confidence on the ratio  $d_i/f_i$  as reported by [32]. If we do not consider the AB+ group in the analysis (N=6), we observe a linear correlation of 0.93 with a p-value of 0.007.

## B. Cases where infection data are not stratified by blood type

### 1. Europe

The quantities  $\pi_T^{(k)}$  represent the inverse of the characteristic time of the infection (of the whole population) at its onset. Therefore, they can be directly compared with the quantities  $m$  previously discussed. Since the slopes  $m$  are measured plotting the data as a function of the

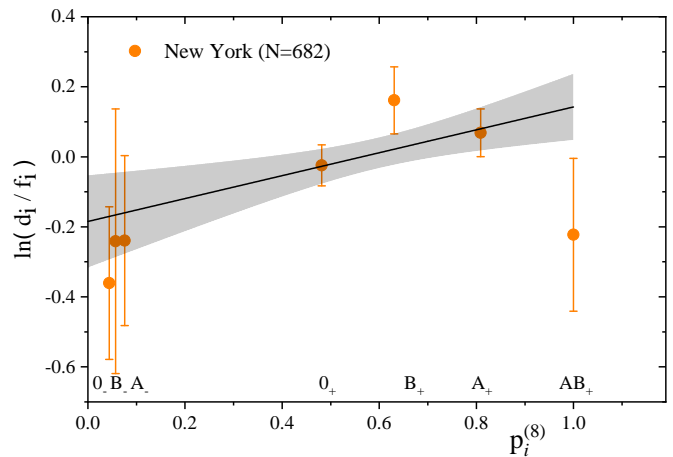


FIG. 5: Ratio between frequencies of infected people for each ABO $\times$ Rh groups (except AB- one),  $d_i$  over frequency of the group on the whole population,  $f_i$  as measured in New York [32] versus its theoretical prediction,  $p_i^{(8)}$  obtained from Eq. (30) using the ABO+Rh set of rules and the blood type frequencies in Table III. Black line represents the best solution of a linear fit.

real-time  $t$ , while  $\pi_T^{(k)}$  are proportional to the scaled time  $\tau = \beta t$ , we expect the relation  $m = \beta \pi_T^{(k)} = \beta p_T^{(k)} - \gamma$ . Therefore, from a plot of  $m$  vs.  $p_T^{(k)}$ , we can both check the validity of the model and extract the parameters  $\beta$  and  $\gamma$ .

At first, we compared the  $m$  found for the 29 countries of the European area with the corresponding  $p_T^{(k)}$ s computed starting from the frequencies of the different blood types found in each country and reported in Table IV. While a contagion scheme based only on the Rhesus group rules ( $p_T^{(2)}$ ) does not explain the observed trends of the epidemics, a high Pearson correlation (0.71) is present between data and model predictions when contagions are driven by the ABO group rules ( $p_T^{(4)}$ ). Indeed, as shown in Figure 6, countries with higher susceptibility also present, on average, a higher  $m$  value. A linear fit of the data allows us to extract the overall values of infection ( $\beta$ ) and recovery ( $\gamma$ ) rates that if combined yield a value of  $R_0$  of  $\sim 2$  in excellent agreement with the current estimates of reproduction number in the early stages of the outbreak [35].

We note that points tend to form two clusters. Interestingly, retrieving the geographic information, we see a clear east-to-west gradient of the susceptibility, which drives back to the different geographical distribution of the ABH phenotypes [36]. Figure 7 clearly shows at a glance this trend for the four-group susceptibility,  $p_T^{(4)}$ .

The addition of the Rhesus information to the ABO scheme ( $p_T^{(8)}$ ) produces a negligible increase of the correlation, while rates remain compatible with those found for  $p_T^{(4)}$  case. To test the obtained linear trends, we performed an F-test assuming a constant slope as null-hypothesis.

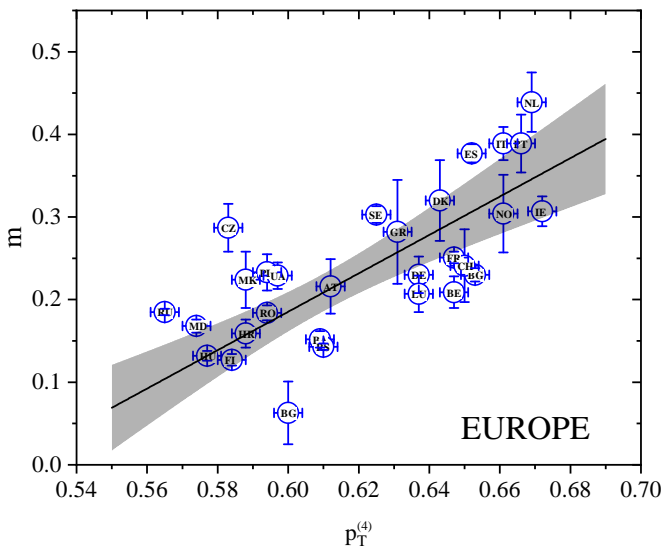


FIG. 6: Inverse characteristic time of the epidemic exponential phase extracted from cumulative infection curves,  $m$ , vs theoretical prediction,  $p_T^{(4)}$  obtained from Eq. (28) using the ABO set of rules and the blood type frequencies in Table IV. Each dot corresponds to one of the 29 analyzed countries in the European region named according to the 2-letter ISO code and reported in Table IV. The black line represents the best solution of a linear fit performed with the York method and the grey shaded area is the  $\pm$  one standard deviation confidence band.

In Table V, p-values for both the Pearson coefficient and F-statistic are reported. Note that the significance of  $p_T^{(2)}$  is just an artifact of the data disposition, which tend to cluster around the values of  $p_T^{(2)} = 0.87$ , thus yielding a high slope. Reversing the axis and repeating the linear fit, one obtains a value of F of 1.28 which has a p-value above the threshold.

## 2. Asia

Repeating the same analyses carried out for European countries with those in the Asia region, we found an overall similar trend, where the major difference lies in the contribution of the Rhesus group. In particular, both  $p_T^{(2)}$  and  $p_T^{(4)}$  values present a non-random linear correlation with the inverse characteristic times,  $m$ , of 0.54 and 0.45, respectively. The corresponding p-values are below the threshold of 0.05 for the 21 Asiatic countries. Interestingly, combining the ABO and Rh rules, the accordance between the observed trend and the theoretical predictions increases up to a correlation value of 0.74, quite similar to the European one. The infection and recovering rates obtained through a linear fit of the data, are slightly higher than those found ruling the infection in Europe although their ratio gives an almost equal  $R_0$ .

Testing the linear fits with the F-test, we can reject the null hypothesis for all three cases, with the usual

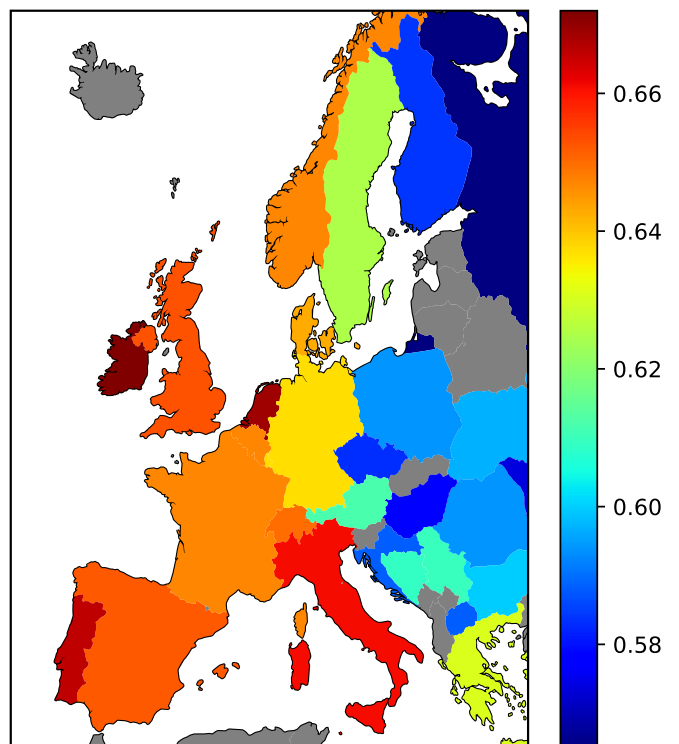


FIG. 7: Map representation of European countries. Each country is colored according to its  $p_T^{(4)}$  susceptibility value obtained from Eq. (28) using the ABO set of rules and the blood type frequencies reported in Table IV.  $p_T^{(4)}$  values increase going from blue to red. Gray countries have not been considered due to a lack of either blood or infection information. The map shows large variability in the susceptibility  $p_T^{(4)}$  (that ranges from 0.56 to 0.68) and a clear east-to-west gradient. The increase of susceptibility going west is a direct consequence of the tendency of increase of the 0 blood type in this direction: the more one blood type dominates, the higher is the susceptibility.

threshold level of 0.05. All results are again summarized in Table V.

## 3. South America and Africa

Finally, we consider two other distinct regions, i.e. South America and Africa, both characterized by a still exponentially proliferating infection. The former exhibits a trend similar to the Europe one, characterized by an un-substantial contribution of the Rhesus group rules, while a correlation of 0.62 is present between the  $m$  coming from the fitting of the infection curves and  $p_T^{(4)}$ . The infection and recovering rates obtained by a linear fit are both smaller than those found in the Eurasian region. However, they combine to give a value of  $R_0$  of  $\sim 2$ . Both the p-value of the Pearson correlation and that an F-test on the linear fit are below the significance threshold of 0.05 for all set of rules except for  $p_T^{(2)}$  one. Results

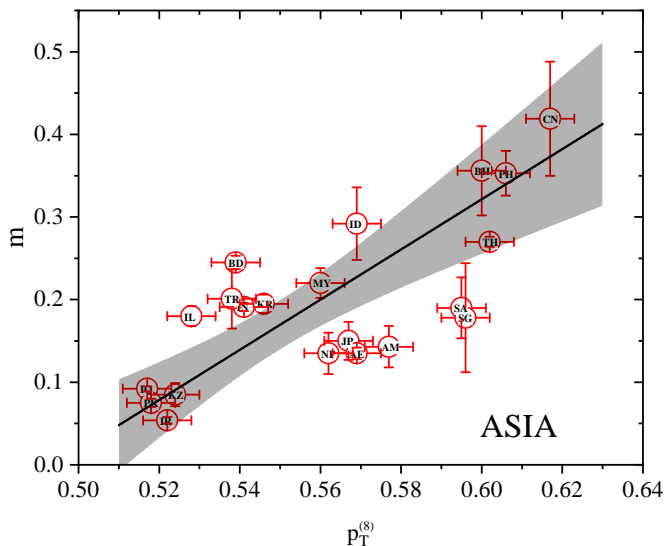


FIG. 8: Inverse characteristic time of the epidemic exponential phase extracted from cumulative infection curves,  $m$  vs theoretical prediction,  $p_T^{(8)}$  obtained from Eq. (28) combining the ABO and  $Rh\pm$  sets of rules and using the blood type frequencies in Table IV. Each dot corresponds to one of the 21 analysed countries in the Asiatic region named according to the 2-letter ISO code and reported in Table IV. Black line represents the best solution of a linear fit.

for the African region instead show no meaningful correlation. As it is the slope of the best linear fit which does not pass an F-test with zero slope as a null hypothesis.

#### 4. Final comments on the countries cases

Overall, we found a statistically significant correlation among the  $m$  and  $p_T^{(k)}$  ( $k = 4, 8$ ) data for Europe, Asia, and South Americas, taken individually. The reason for analyzing separately these continents lies in the fact that we expect that beside blood type distribution other factors affect the infectivity onset and initial growth rate. The lifestyle and the local climate are certainly some of them. We have therefore considered countries aggregations that preserve at the best these two aspects. To check this hypothesis, we have analyzed (see Table VI) what is the effect of adding North America and/or Australia to the European countries. As can be seen in Table VI, the Pearson correlation does not change significantly in these cases. A rather worst result is obtained by considering Asia and Europe together, although the Pearson correlation still maintains a high degree of statistical significance (p-value better than  $10^{-4}$ ). The correlation becomes even worst when considering the whole world (Pearson 0.43) but also in this case there is a great advantage (p-value better than  $10^{-3}$ ) with respect to the null hypothesis (no-correlation between  $m$  and  $p_T^{(k)}$ ). We conclude that the model presented here is compatible with the existing data.

As far as the effect of temperature, humidity, etc. it is tempting to speculate on the obtained results: *i*) Europe and Asia share a good correlation, as well as the values of  $\beta$  and  $\gamma$ ; *ii*) South America has again a good correlation, but its  $\beta$  and  $\gamma$  are smaller than in Europe and Asia; *iii*) Africa shows a bad correlation. These three points could be rationalized remembering that, at the pandemic onset Europe and Asia were in their wintertime, South America in the summertime, while African countries experienced different climate situations.

## V. DISCUSSION

Most of the proteins that decorate cell membranes are bound to glycans [37]. The presence of those carbohydrate chains provides a further channel of interaction between proteins, besides the usual direct protein-protein one, and evolved to play a large array of life-sustaining functions including support, signaling, protein folding, and protection.

It has been suggested that protection against pathogens was the driving force that favored the evolution of the complex landscape of glycan interactions (see e.g. [38] for a more detailed discussion).

Since viruses do not have genes for glycan synthesis or modification, they inherit host cell glycans after each round of replication in a new host. This means that the host cell in which the virus last replicated generated the glycans on viral glycoproteins [38].

A mutation in the host population having as an outcome the loss of a glycan modification could then provide a selective advantage to the glycan-lacking subpopulation. In fact, pathogens using that glycan as a receptor would not be able to invade the host cells anymore. Moreover, the host can develop specific antibodies against the abolished glycan [39].

Human blood groups constitute an important example. Individuals having O blood group lack of A or B antigens and when presented with glycan motifs similar to either A or B antigens, they develop anti-A and anti-B antibodies. Individuals with A or B blood group develop either anti-B or anti-A antibodies, respectively. On the other hand, people with subgroup AB lack such antibodies.

According to those ‘rules’, in case of an infection, one would expect that looking at the blood type of the people found infected by the virus, group O should be under-represented with respect to its occurrence in the whole population. This feature has been indeed observed by Zhao and coworkers [18] for the COVID-19 outbreak, caused by the novel SARS-CoV-2 coronavirus. Notably, a similar behavior was found in the hospital outbreak of SARS in Hong Kong in 2003 [40]. Moreover, both SARS-CoV and SARS-CoV-2 S protein trimers are covered by an extensive glycan shield, surrounding the receptor-binding domain and can infect cells that express ABH antigens according to the individual phenotype [41, 42].

Importantly, the dilution effect on the contagion due to

TABLE V: Main results for the different countries aggregation.

Continent		$\beta$	$\gamma$	$\rho$	Pearson p-value	F	p-value
Europe (EU) (29 countries)	$p_T^{(2)}$	-35.39	-31.01	-	-0.26	0.17	$22.4 < 10^{-4}$
	$p_T^{(4)}$	2.31	1.20	0.52	0.71	$< 10^{-4}$	$42.5 < 10^{-4}$
	$p_T^{(8)}$	3.36	1.57	0.48	0.71	$< 10^{-3}$	$34.2 < 10^{-4}$
Asia (AS) (21 countries)	$p_T^{(2)}$	2.06	1.80	-	0.54	0.01	$19.5 < 10^{-3}$
	$p_T^{(4)}$	4.42	2.38	0.54	0.45	0.04	1.3 0.05
	$p_T^{(8)}$	3.02	1.49	0.49	0.74	$< 10^{-3}$	$39.2 < 10^{-4}$
South America (SA) (13 countries)	$p_T^{(2)}$	-0.46	-0.62	-	0.29	0.34	0.79 0.39
	$p_T^{(4)}$	1.24	0.67	0.54	0.62	0.02	8.1 0.02
	$p_T^{(8)}$	1.13	0.55	0.49	0.58	0.04	6.7 0.03
Africa (AF) (12 countries)	$p_T^{(2)}$	0.37	0.25	0.74	-0.09	0.78	0.5 0.5
	$p_T^{(4)}$	0.52	0.22	0.42	-0.07	0.82	1.2 0.3
	$p_T^{(8)}$	0.38	0.11	0.29	0.01	0.97	1.2 0.3

TABLE VI: Pearson correlations between  $m$  and  $p_T^{(k)}$  ( $k = 4, 8$ ) for different continent aggregations.

Aggregation	Countries	$p_T^{(k)}$	Pearson	p-value
Europe and North America	31	$p_T^{(4)}$	0.70	$< 10^{-4}$
		$p_T^{(8)}$	0.70	$< 10^{-4}$
Europe and Australia	30	$p_T^{(4)}$	0.69	$< 10^{-4}$
		$p_T^{(8)}$	0.70	$< 10^{-4}$
Europe and Asia	50	$p_T^{(4)}$	0.62	$< 10^{-4}$
		$p_T^{(8)}$	0.58	$< 10^{-4}$
Temperate (North)	48	$p_T^{(4)}$	0.63	$< 10^{-4}$
		$p_T^{(8)}$	0.51	$< 10^{-3}$
Tropical	26	$p_T^{(4)}$	0.24	0.24
		$p_T^{(8)}$	0.31	0.12
Temperate (Sud)	4	$p_T^{(4)}$	0.97	0.03
		$p_T^{(8)}$	0.94	0.06
World	78	$p_T^{(4)}$	0.43	$< 10^{-3}$
		$p_T^{(8)}$	0.34	0.002

the asymmetrical transmissions must be reflected in the growth of the epidemics. In the present work, we have studied how the existence of asymmetrical virus transmissions affect such growth.

To this aim, we expanded the usual SIR formalism to take into consideration the possible effect of blood antigenicity in the COVID-19 transmission, which closely resembles that of blood transfusions. To solve the set of generalized SIR Equations (16)-(18) for any time, one has to rely on numerics, however, we provided analytical solutions in the small-time limit, where the epidemics is in its exponential-growing regime. In particular, we obtained an expression linking the inverse characteristic time of the exponential phase with the abundances of the different blood groups in the population. We propose a set of susceptibility indices:  $p_i^{(k)}$  for the sub-population  $i$  and  $p_T^{(k)}$  for the total population. Here  $k=2$  accounts

for only the Rh $\pm$  system,  $k=4$  for the ABO system, and  $k=8$  for the ABO $\times$ Rh $\pm$  one. The model predicts a linear dependence of the observed epidemic inverse timescale  $m$  with the total susceptibility.

To test the model, we first compare its predictions with the experimental data provided in [18], where the blood type of infected people of two Chinese regions was collected. Comparing the population frequencies of blood groups with those found in the infected sub-population, we verified that the proposed contagion scheme well describes the observed frequencies, since the difference observed between the ABO blood type population distribution and the ABO blood type infected people distribution supports the validity of the infection scheme proposed in [1]. A similar approach has been used to test the model for two further cases (Ankara [31] and New York [32]) where data are available, although with a much lower statistic. Albeit the low statistical confidence of the provided data, both cases seem in qualitative agreement with the model prediction.

Unfortunately, besides the data analyzed in [18, 31, 32], which are restricted to the Wuhan/Shenzhen, New York, and Ankara regions, respectively, no large-scale data are available about the distribution on the blood type of infected people.

Then we analyzed the infection curves of a large set of countries worldwide, comparing the characteristic time of the infection outbreak with the prediction of our model based on the known blood group distribution for each country. This allows us to discard possible bias due to data collection and geographical factors. Note that in this second case, we do not have the information about the blood groups of the infected population but only on the whole population. Thus, we can compare the growth rate in the short time, exponential, phase with the ‘‘susceptibility’’  $p_T^{(k)}$  proposed by the model.

We managed to collect data on the blood frequencies and the infections for 78 different countries belonging to a well distinct geographical area, i.e. Europe, Asia, South America, and Africa. Since we expect that differences

both geographical and on the lifestyles affect the infection and recovering rates we kept the countries separated according to the four identified areas.

Rhesus blood types have a marked effect in the Asiatic countries, which are characterized by a broad distribution of  $p_T^{(2)}$ . On the other hand, Europe and South America present a narrower distribution. Anyhow, the correlation measured using the  $k=2$  susceptibility turns out to be always not significant. As far as the  $k=4$  and  $k=8$  case, three out of the four areas present a very good agreement between data and model prediction (see Table V). The  $k=8$  case is better than  $k=4$  in Asia, while no substantial difference is found in Europe and South America (mainly because of the lower abundance of Rh– with respect to Asia). Summing up, it seems that the best agreement between data and model is found for  $k=8$ : both ABO and Rh± blood type have an effect on the virus spreading pattern.

In a nutshell, we proposed a generalized SIR model with infection rules dictated by antigenicity between different blood types. Obtaining an analytical solution of the model for the exponential phase, we were able to provide a rigorous theoretical test of the hypothesis proposed

in [1]. We have made the test both for local data, where the number of infected people is stratified by blood type, and, on a wider scale, analyzing the infection growth curves of 78 counties worldwide. Overall, the present study reaches the conclusion that the hypothesis of a blood type effect on the COVID-19 advanced in [1] it is not falsified by the available observational epidemic data.

Obviously, to strengthen the validation of the hypothesis in [1] a direct detection of the antigens linked to the SARS-CoV-2 is needed, but this goes far beyond the goals of the present paper.

As a final note, we observe that, besides blood types, other population dependent antigens distribution could play a role in the geographically heterogeneous infection spreading [43].

### Conflict of Interest Statement

The authors declare that the research was conducted in the absence of any commercial or financial relationships that could be construed as a potential conflict of interest.

- 
- [1] A. Breiman, N. Ruv en-Clouet, and J. Le Pendu, *PLoS Pathogens* **16**, e1008556 (2020).
- [2] C. Wang, P. W. Horby, F. G. Hayden, and G. F. Gao, *The Lancet* **395**, 470 (2020).
- [3] C. Huang, Y. Wang, X. Li, L. Ren, J. Zhao, Y. Hu, L. Zhang, G. Fan, J. Xu, X. Gu, et al., *The Lancet* **395**, 497 (2020).
- [4] N. Zhu, D. Zhang, W. Wang, X. Li, B. Yang, J. Song, X. Zhao, B. Huang, W. Shi, R. Lu, et al., *New England Journal of Medicine* (2020).
- [5] The 2019-nCoV Outbreak Joint Field Epidemiology Investigation Team and Q. Li, *China CDC Weekly* **2**, 79 (2020).
- [6] Anon., *WHO Director-General’s opening remarks at the media briefing on COVID-19 - 11 March 2020*.
- [7] A. C. Walls, Y.-J. Park, M. A. Tortorici, A. Wall, A. T. McGuire, and D. Veesler, *Cell* (2020).
- [8] R. M. Anderson and R. M. May, *Nature* **280**, 361 (1979).
- [9] B. Mart nez-L pez, B. Ivorra, A. Ramos, and J. M. S nchez-Vizca no, *Veterinary microbiology* **147**, 300 (2011).
- [10] K. Prem, Y. Liu, T. W. Russell, A. J. Kucharski, R. M. Eggo, N. Davies, M. Jit, P. Klepac, S. Flasche, S. Clifford, et al., *The Lancet Public Health* **5**, e261 (2020).
- [11] M. B. Araujo and B. Naimi, *medRxiv* p. 2020.03.12.20034728 (2020).
- [12] K. M. O’Reilly, M. Auzenbergs, Y. Jafari, Y. Liu, S. Flasche, and R. Lowe, *Effective transmission across the globe: the role of climate in COVID-19 mitigation strategies* (2020).
- [13] A. Amoroso, A. Vintzileos, F. Miralles-Wilhelm, M. M. Sajadi, P. Habibzadeh, and S. Shokouhi, *SSRN Electronic Journal* (2020).
- [14] N. Scafetta, *International Journal of Environmental Research and Public Health* **17**, 3493 (2020).
- [15] G. Sebastiani, M. Massa, and E. Riboli, *European Journal of Epidemiology* **35**, 341 (2020).
- [16] K. N. Kershaw, A. V. D. Roux, M. Carnethon, C. Darwin, D. C. Goff, W. Post, P. J. Schreiner, and K. Watson, *American Journal of Hypertension* **23**, 46 (2010).
- [17] H. Samouda, M. Ruiz-Castell, V. Bocquet, A. Kuemmerle, A. Chioti, F. Dadoun, N.-B. Kandala, and S. Stranges, *PLOS ONE* **13**, e0197021 (2018).
- [18] J. Zhao, Y. Yang, H.-P. Huang, D. Li, D.-F. Gu, X.-F. Lu, Z. Zhang, L. Liu, T. Liu, Y.-K. Liu, et al., *medRxiv* (2020).
- [19] P. Guillon, M. Cl ment, V. S bille, J.-G. Rivain, C.-F. Chou, N. Ruvo en-Clouet, and J. Le Pendu, *Glycobiology* **18**, 1085 (2008).
- [20] A. Vespignani, *Nature physics* **8**, 32 (2012).
- [21] B. Ivorra, M. R. Ferr andez, M. Vela-P rez, and A. Ramos, *Communications in nonlinear science and numerical simulation* p. 105303 (2020).
- [22] K. Roosa, Y. Lee, R. Luo, A. Kirpich, R. Rothenberg, J. Hyman, P. Yan, and G. Chowell, *Infectious Disease Modelling* **5**, 256 (2020).
- [23] A. J. Kucharski, T. W. Russell, C. Diamond, Y. Liu, J. Edmunds, S. Funk, R. M. Eggo, F. Sun, M. Jit, J. D. Munday, et al., *The lancet infectious diseases* (2020).
- [24] Z. Yang, Z. Zeng, K. Wang, S.-S. Wong, W. Liang, M. Zanin, P. Liu, X. Cao, Z. Gao, Z. Mai, et al., *Journal of Thoracic Disease* **12**, 165 (2020).
- [25] Q. Lin, S. Zhao, D. Gao, Y. Lou, S. Yang, S. S. Musa, M. H. Wang, Y. Cai, W. Wang, L. Yang, et al., *International journal of infectious diseases* (2020).
- [26] M. S. Boudrioua and A. Boudrioua (2020).
- [27] G. C. Calafiore, C. Novara, and C. Possieri (2020).
- [28] B. Tang, X. Wang, Q. Li, N. L. Bragazzi, S. Tang,



- Y. Xiao, and J. Wu, *Journal of clinical medicine* **9**, 462 (2020).
- [29] A. Menon, N. K. Rajendran, A. Chandrachud, and G. Setlur (2020).
- [30] R. Anderson, B. Anderson, and R. May, *Infectious Diseases of Humans: Dynamics and Control*, Dynamics and Control (OUP Oxford, 1992), ISBN 9780198540403.
- [31] H. Goker, E. Aladag Karakulak, H. Demiroglu, C. M. Ayaz Ceylan, Y. Buyukasik, A. C. Inkaya, S. Aksu, N. Sayinalp, I. C. Haznedaroglu, O. Uzun, et al., *Turkish journal of medical sciences* (2020).
- [32] M. Zietz and N. P. Tatonetti (2020).
- [33] Wikipedia, *Blood type distribution by country* (2020), [Online; checked the 11th of June 2020], URL [https://en.wikipedia.org/w/index.php?title=Blood\\_type\\_distribution\\_by\\_country&oldid=961584410](https://en.wikipedia.org/w/index.php?title=Blood_type_distribution_by_country&oldid=961584410).
- [34] G. W. H. Organization, *Who coronavirus disease (covid-19) dashboard* (2020), [Online; downloaded the 12th of June 2020], URL <https://covid19.who.int/>.
- [35] A. J. Kucharski, T. W. Russell, C. Diamond, Y. Liu, J. Edmunds, S. Funk, R. M. Eggo, F. Sun, M. Jit, J. D. Munday, et al., *The Lancet Infectious Diseases* **20**, 553 (2020).
- [36] A. E. Mourant and I. M. Watkin, *Heredity* **6**, 13 (1952).
- [37] A. Varki, *Glycobiology* **27**, 3 (2016).
- [38] J. R. Bishop and P. Gagneux, *Glycobiology* **17**, 23R (2007), ISSN 0959-6658.
- [39] P. Patel and J. F. Kearney, *The Journal of Immunology* **197**, 4201 (2016).
- [40] Y. Cheng, G. Cheng, C. H. Chui, F. Y. Lau, P. K. S. Chan, M. H. L. Ng, J. J. Y. Sung, and R. S. M. Wong, *JAMA* **293**, 1447 (2005).
- [41] J. Chen and K. Subbarao, *Annual Review of Immunology* **25**, 443 (2007).
- [42] Y. Watanabe, Z. T. Berndsen, J. Raghvani, G. E. Seabright, J. D. Allen, O. G. Pybus, J. S. McLellan, I. A. Wilson, T. A. Bowden, A. B. Ward, et al., *Nature Communications* **11** (2020).
- [43] As an example, it is worth to note that the distribution of the HLA types is highly variable in Europe. It is suggestive to consider that HLA-DRB1\*11:01 shows a large peak in the northern Italian regions, where the epidemic has been by far more severe than in the rest of the continent.